



Synthesis, spectroscopic characterization, catalytic and antibacterial studies of ruthenium(III) Schiff base complexes



A.F. Shoair*, A.R. El-Shobaky, H.R. Abo-Yassin¹

Department of Chemistry, Faculty of Science, Damietta University, Damietta 34517, Egypt

ARTICLE INFO

Article history:

Received 30 January 2015

Received in revised form 30 May 2015

Accepted 1 July 2015

Available online xxxx

Keywords:

Schiff base

Ruthenium(III)

Catalytic oxidation

Antibacterial

ABSTRACT

The bidentate Schiff base ligands (**HL_n**) have been synthesized by condensation of 2-hydroxy-1-naphthaldehyde with aniline and its *p*-substituted derivatives in ethanol. Ruthenium(III) complexes of the type [Ru(L_n)₂(H₂O)₂]Cl have been synthesized by the reaction of RuCl₃·nH₂O with the Schiff base ligands (in a molar ratio 1:2) in ethanol. The ligands and their Ru(III) complexes have been characterized by elemental analysis, magnetic susceptibility, spectroscopic (FTIR, UV–vis, ¹H NMR and X-ray diffraction) and thermal analysis techniques. All the ruthenium(III) complexes are found to be stable, paramagnetic, low spin and octahedrally coordinated by the ligands through the nitrogen atom of the azomethine (–C=N–) group and the oxygen atom of the deprotonated phenolic group. The molecular and electronic structures of the investigated ligands (**HL_n**) were also studied using quantum chemical calculations. The complexes (**1**, **3** and **5**) exhibited a catalytic activity for the oxidation of benzoin to benzil with moderate to high yield in the presence of sodium periodate as co-oxidant. The antibacterial activities of the ligands (**HL_n**) and their Ru(III) complexes towards Gram positive and Gram negative bacteria have been investigated.

© 2015 Elsevier B.V. All rights reserved.

1. Introduction

Schiff bases form an interesting class of chelating ligands that has enjoyed popular use in the coordination chemistry of transition elements [1,2]. A large number of Schiff bases and their metal complexes have been studied because of their interesting and important properties such as their ability to reversibly bind oxygen and their use in catalyses [3,4] and biological systems [5,6]. Aromatic Schiff bases with an *o*-hydroxy substituent possess a very interesting characteristic-reversible color changes induced by irradiation (photochromism) or by a change in temperature (thermochromism). The change of color of thermochromic compounds is ascribed to the tautomerism between the OH and NH groups resulting from intramolecular hydrogen transfer between an enolimine and ketoamine tautomer, which can be *cis* or *trans* relative to the C=N bond [7]. We have reported a number of ruthenium complexes containing N,O-donor ligands and investigated their catalytic activity for alcohol oxidation in combination with various oxidants such as K₂S₂O₈, IO(OH)₅, H₂O₂ and NMO [8–11]. Recently, we have synthesized a new class of ruthenium(III) complexes, [Ru^{III}Cl(L)₂(H₂O)] and [Ru^{III}Cl₂(L)₂]Cl (L = 2-aminophenol, 8-hydroxyquinoline and 4-aminoantipyrine). Elemental analysis and spectroscopic characterization showed an octahedral geometry around ruthenium(III) ion [12].

In continuation of our earlier work [13,14], we report the synthesis and characterization of the Schiff base ligands (**HL_n**) derived from the condensation of 2-hydroxy-1-naphthaldehyde with aniline and its *p*-substituted derivatives. Their ruthenium(III) complexes were synthesized and characterized by different spectroscopic techniques. The optimized bond lengths, bond angles and the calculated quantum chemical parameters for the ligands (**HL_n**) were investigated. Also, we investigated the catalytic activity of these complexes towards the oxidation of benzoin to benzil at different temperatures. The antibacterial activities of the ligands and their Ru(III) complexes towards Gram positive and Gram negative bacteria have been investigated.

2. Experimental

2.1. Chemicals and physical measurements

All the chemicals and solvents were purchased from Sigma-Aldrich Chemicals Company (USA) and used without further purification. Microanalytical data (C, H and N) were collected on Automatic Analyzer CHNS Vario ELIII, Germany. Spectroscopic data were obtained using the following instruments: FTIR spectra (KBr disks, 4000–400 cm⁻¹) by Jasco FTIR-4100 spectrophotometer; the ¹H NMR spectra by Bruker WP 300 MHz using DMSO-d₆ as a solvent containing TMS as the internal standard. UV–visible spectra by Perkin-Elmer AA800 spectrophotometer Model AAS. Thermal analysis of the Schiff base ligands and their Ru(III) complexes were carried out using a Shimadzu thermogravimetric analyzer under a nitrogen atmosphere with heating rate of 10 °C/min

* Corresponding author.

E-mail address: abdel_shoair@yahoo.com (A.F. Shoair).

¹ Abstracted from her M.Sc. Thesis.

over a temperature range from room temperature up to 800 °C. Magnetic susceptibility measurements were determined at room temperature on a Johnson Matthey magnetic susceptibility balance using $\text{Hg}[\text{Co}(\text{SCN})_4]$ as calibrant. Conductivity measurements of the complexes at 25 ± 1 °C were determined in DMF (10^{-3} M) using conductivity/TDS meter model Lutron YK-22CT. X-ray diffraction analysis of compounds were recorded on X-ray diffractometer in the range of diffraction angle $2\theta = 8\text{--}40^\circ$. This analysis was carried out using $\text{CuK}\alpha$ radiation ($\lambda = 1.54098$ Å). The applied voltage and the tube current are 40 kV and 30 mA, respectively. The molecular structures of the investigated compounds were optimized by HF method with 3-21G basis set. The molecules were built with the Perkin Elmer ChemBio Draw and optimized using Perkin Elmer ChemBio3D software [15].

2.2. Preparation of Schiff base ligands (HL_n)

The Schiff base ligands (HL_n) were prepared (Fig. 1) by ethanolic solution of 2-hydroxy-1-naphthaldehyde (20 mmol in 15 cm^3 of ethanol) to ethanolic solution of aniline and its *p*-derivatives (20 mmol, 15 cm^3) of ethanol. The mixture was refluxed for 4 h with stirring, during this time yellow to orange precipitates are formed. The precipitates were collected by filtration, washed twice with hot ethanol and dried in a vacuum desiccator over anhydrous CaCl_2 .

The resulting formed ligands are:

HL₁	2-hydroxy-1-naphthylidene-4-methoxyaniline
HL₂	2-hydroxy-1-naphthylidene-4-methylaniline
HL₃	2-hydroxy-1-naphthylideneaniline
HL₄	2-hydroxy-1-naphthylidene-4-chloroaniline
HL₅	2-hydroxy-1-naphthylidene-4-nitroaniline.

2.3. Preparation of ruthenium(III) Schiff base complexes (1–5)

All Ru(III) complexes (1–5) (Fig. 2) were synthesized according to the general procedure [13]: a stoichiometric amount of the desired ligand (2 mmol, 20 cm^3) in ethanol was added dropwisely to a hot ethanolic solution of $\text{RuCl}_3 \cdot n\text{H}_2\text{O}$ (1 mmol, 20 cm^3) with stirring and the reaction mixture was refluxed for 3 h. The solution was

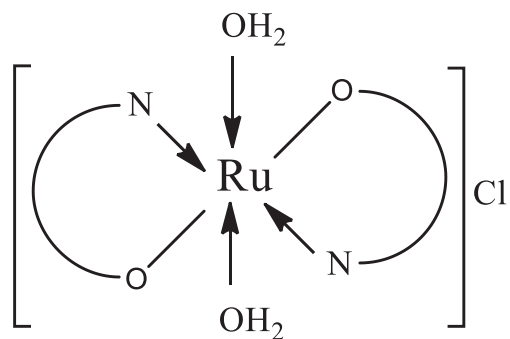


Fig. 2. The proposed structure of the complexes (1–5) $[\text{Ru}(\text{L}_n)_2(\text{H}_2\text{O})_2]\text{Cl}$.

concentrated to half of its original volume by evaporation and allowed to cool at room temperature. During this, a microcrystalline solid was separated, which was isolated by filtration, washed with hot ethanol, ether and dried in a vacuum desiccator over anhydrous Na_2SO_4 .



2.4. Catalytic oxidation of benzoin by ruthenium(III) complexes

The complex $[\text{Ru}(\text{L}_n)_2(\text{H}_2\text{O})_2]\text{Cl}$ ($n = 1, 3$ or 5) was dissolved in a mixture of 5 cm^3 of DMF and 5 cm^3 CH_3CN (0.01 mmol). To which benzoin (2 mmol) was added with stirring, then an aqueous solution of NaIO_4 (5 mmol, 5 ml water) was added dropwisely within half an hour and the reaction mixture was further stirred for 4 h at 70 °C. The reaction mixture was extracted with diethyl ether to collect benzil and dried over anhydrous Na_2SO_4 and weighed.

2.5. Antibacterial investigation

In vitro antibacterial activity studies were carried out using the standardized disk-agar diffusion method [16] to investigate the inhibitory effect of the synthesized Schiff base ligand and their Ru(III) complexes

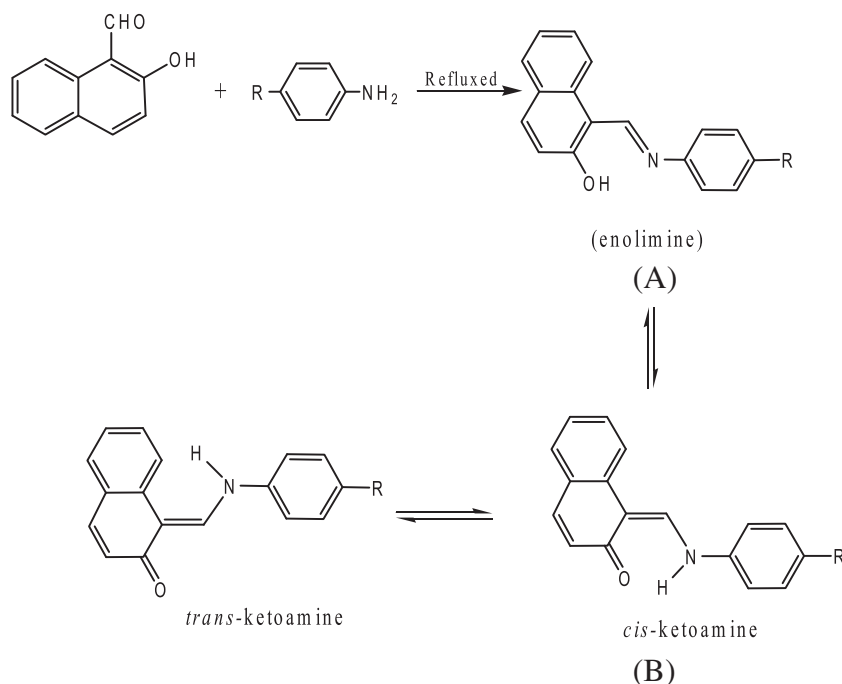


Fig. 1. The structure of the Schiff base ligands (HL_n).

against Gram-positive bacteria (e.g., *Bacillus cereus* and *Staphylococcus aureus*) Gram-negative bacteria (e.g., *Escherichia coli* and *Klebsiella pneumoniae*) as a kind of fungi. An inhibition zone diameter indicates that the tested compounds are active against the used kinds of the bacteria and fungus. The tested compounds were dissolved in DMF (which have no inhibition activity). Also, the antifungal activities were tested against four local fungal species (*Aspergillus niger*, *Alternaria alternata*, *Penicillium italicum* and *Fusarium oxysporium*) on DOX agar medium. The concentrations of each solution were 50, 100 and 150 µg/ml. By using a sterile cork borer (10 mm diameter), wells were made in agar medium plates previously seeded with the test microorganism. 200 µl of each compound was applied in each well. The agar plates were kept at 4 °C for at least 30 min to allow the diffusion of the compound to agar medium. The plates were then incubated at 37 °C or 30 °C for bacteria and fungi, respectively. The diameters of inhibition zone were determined after 24 h and 7 days for bacteria and fungi, respectively, taking the consideration of the control values (DMF). Penicillin and miconazole were used as reference substances against bacteria and fungi, respectively.

3. Results and discussion

The results of physical properties of the prepared ligands (**HL_n**) and their Ru(III) complexes (**1–5**) along with their elemental analysis are collected in Table 1. The analytical data of Ru(III) complexes indicated that the complexes have 1:2 (metal:ligand) stoichiometry. The complexes of the type [Ru(**L_n**)₂(H₂O)₂]Cl (where **L_n** = mono anion of the bidentate Schiff base ligands) are stable in air and soluble in most common organic solvents. All the complexes are soluble in highly coordinating solvents like DMSO and DMF. The ligands are asymmetrical bidentate and coordinate through the nitrogen atom of the azomethine (–C=N–) group and the oxygen atom of the deprotonated phenolic group. Hence, the complexes [Ru(**L_n**)₂(H₂O)₂]Cl have a D_{2h}-symmetry (Fig. 2). The composition of these complexes has been confirmed by elemental analysis and spectroscopic and thermal techniques. The molar conductance values of the Ru(III) complexes (10^{–3} M) are measured in DMF and these values are (51–59 Ω^{–1} cm² mol^{–1}) range indicating the electrolytic nature of the complexes (presence of Cl ion) [1]. The magnetic susceptibility measurements show that the complexes [Ru(**L_n**)₂(H₂O)₂]Cl are paramagnetic (μ_{eff} = 1.8–2.1 BM, low spin d⁵, S = ½), as is normal for ruthenium(III) complexes in an octahedral environment [13].

3.1. Molecular structure of the ligands

The selected geometrical structures of the investigated ligands are calculated by optimizing their bond lengths and bond angles. The calculated molecular structures for ligands tautomers (**A** & **B**) are shown in Fig. 3. Both the highest occupied molecular orbital (HOMO) and lowest

unoccupied molecular orbital (LUMO) are the main orbitals take part in chemical stability. The HOMO represents the ability to donate an electron, LUMO as an electron acceptor represents the ability to obtain an electron. The HOMO and LUMO for ligands tautomers (**A**) are shown in Fig. S1 in the supplementary. The calculated quantum chemical parameters are given in Table 2. Additional parameters such as ΔE, absolute electronegativities, χ, chemical potentials, Pi, absolute hardness, η, absolute softness, σ, global electrophilicity, ω, global softness, S, and additional electronic charge, ΔN_{max}, have been calculated [15] according to the following Eqs. (1)–(8):

$$\Delta E = E_{\text{LUMO}} - E_{\text{HOMO}} \quad (1)$$

$$\chi = \frac{-(E_{\text{HOMO}} + E_{\text{LUMO}})}{2} \quad (2)$$

$$\eta = \frac{E_{\text{LUMO}} - E_{\text{HOMO}}}{2} \quad (3)$$

$$\sigma = \frac{1}{\eta} \quad (4)$$

$$P_i = -\chi \quad (5)$$

$$S = \frac{1}{2\eta} \quad (6)$$

$$\omega = \frac{P_i^2}{2\eta} \quad (7)$$

$$\Delta N_{\text{max}} = -\frac{P_i}{\eta} \quad (8)$$

The HOMO–LUMO energy gap, ΔE, which is an important stability index, is applied to develop theoretical models for explaining the structure and conformation barriers in many molecular systems [15]. The calculations indicated that the form (**A**) is more stable form and highly reactive than form (**B**).

3.2. Infrared spectra

The FTIR spectral data of the Schiff base ligands (**HL_n**) and their Ru(III) complexes (**1–5**) are listed in Table S1 in the supplementary. On the basis of the similarity of the spectra of the complexes (**1–5**), it may be assumed that they have the similar coordination structures. Comparison of the IR spectra of Ru(III) complexes with that of the free Schiff base ligands revealed that:

- (1) The IR spectra of Schiff base ligands exhibited a broad band of medium intensity at the regions 3424–3445 cm^{–1}, strong band at 1607–1619 cm^{–1}, and a medium band at 1230–1255 cm^{–1}, which were assigned to H-bonded OH stretching ν(OH), azomethine ν(C=N) group and phenolic oxygen ν(C–O) group vibrations, respectively.
- (2) The broad band due to ν(OH) group which appear in the spectra of the free ligands at 3424–3445 cm^{–1} region, which associated with the complexes are confirmed by elemental and thermal analyses for the coordinated or uncoordinated water molecules.
- (3) The strong band at 1607–1619 cm^{–1} region assigned to ν(C=N) in the free ligands were shifted to the lower frequencies by 20–25 cm^{–1} indicating the participation of the azomethine group in chelation [17,18].
- (4) Furthermore, on complexation, the medium band corresponding to phenolic oxygen ν(C–O) in the free ligands is shifted to higher wavenumber in the range 1245–1265 cm^{–1} for all the complexes indicating that, the ligands coordinate through their deprotonated form and formation of metal–oxygen bonds.

Table 1

Physical properties and elemental analysis data of Schiff base ligands (**HL_n**) and their Ru(III) complexes (**1–5**).

Compound	M.p. (°C)	Yield%	μ _{eff} (BM)	% found (calc.)		
				C	H	N
HL₁	110	54.17	–	77.78(77.98)	5.28(5.42)	4.77(5.05)
(1) [Ru(L₁) ₂ (H ₂ O) ₂]Cl	126	45.06	1.95	59.48(59.62)	3.76(3.86)	3.57(3.86)
HL₂	122	78.69	–	82.66(82.76)	5.65(5.75)	5.07(5.36)
(2) [Ru(L₂) ₂ (H ₂ O) ₂]Cl	175	40.12	2.01	62.19(62.38)	3.89(4.04)	3.77(4.04)
HL₃	240	17.62	–	82.45(82.59)	5.15(5.26)	5.44(5.67)
(3) [Ru(L₃) ₂ (H ₂ O) ₂]Cl	130	29.33	2.09	61.25(61.39)	3.54(3.61)	3.88(4.21)
HL₄	140	65.91	–	72.34(72.47)	4.14(4.26)	4.76(4.97)
(4) [Ru(L₄) ₂ (H ₂ O) ₂]Cl	120	51.64	1.99	55.54(55.62)	2.77(3.00)	3.64(3.82)
HL₅	220	73.55	–	69.76(69.86)	3.89(4.11)	9.34(9.59)
(5) [Ru(L₅) ₂ (H ₂ O) ₂]Cl	96	62.96	2.10	53.87(54.07)	2.86(2.92)	7.32(7.42)

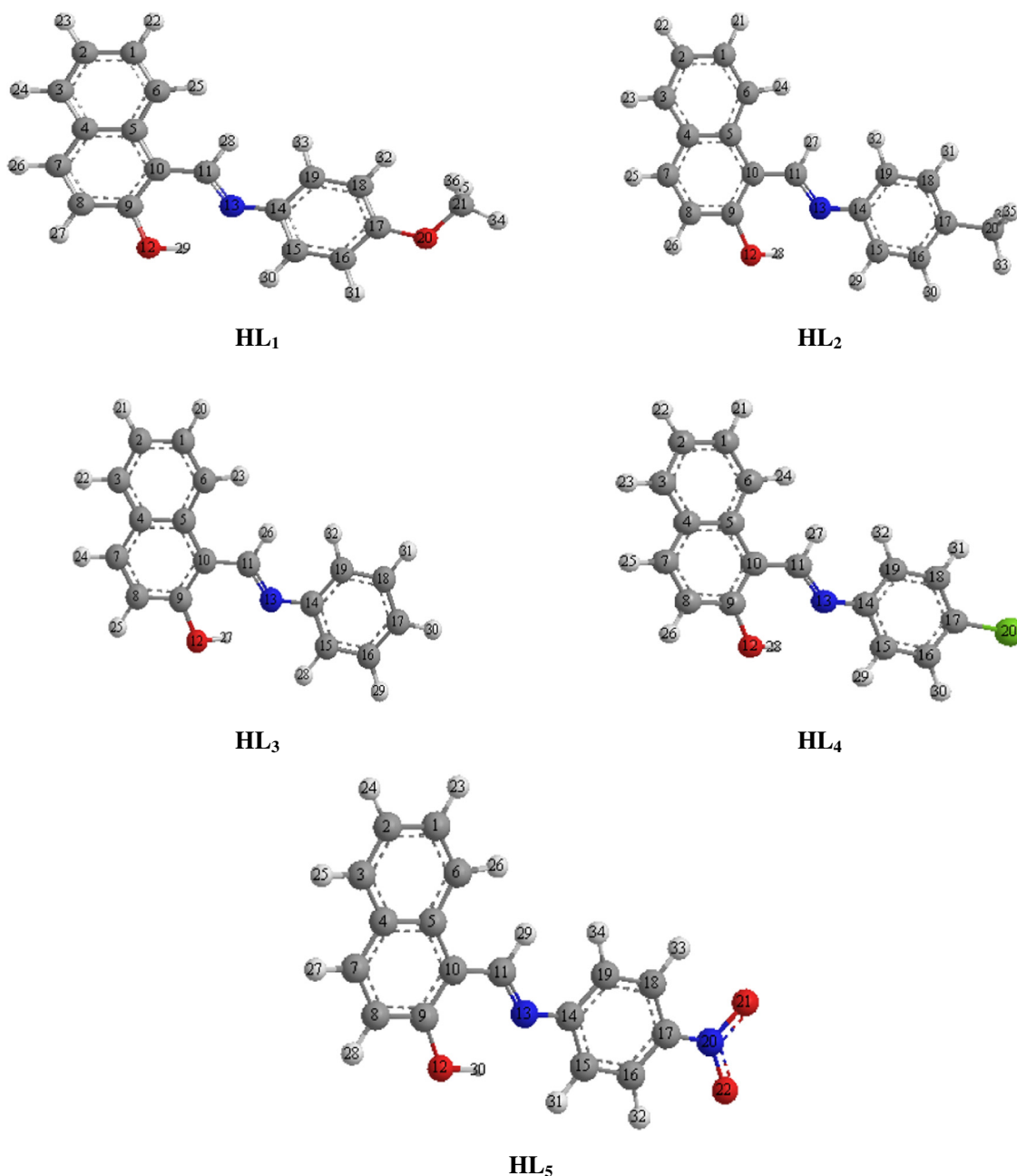


Fig. 3. The calculated molecular structures of the investigated ligands (HL_n).

- (5) In addition, new bands were observed in the region 526–545 and 474–482 cm^{-1} , which were assigned to the formation of $\nu(\text{Ru}-\text{O})$ and $\nu(\text{Ru}-\text{N})$, respectively [19] which further supports the coordination of the azomethine nitrogen and the phenolic oxygen.
- (6) Finally, the presence of coordinated water was suggested by the very broad absorption band in the region 3405–3440 cm^{-1} in the IR spectra of complexes [20].

3.3. ^1H NMR spectra

The ^1H NMR spectra of Schiff base ligands (HL_n) were recorded in d_6 -DMSO at room temperature. The ^1H NMR spectral data showed a multiplet signal of the aromatic protons (m, Ar-H) at 6.90–7.57 and 7.27–7.94 ppm regions of naphthalene and benzene rings, respectively. In the meantime, the ^1H NMR of the HL_1 and HL_2 exhibits signals at

δ (ppm) 3.73 (s, 3H, OCH_3) and 2.35 (s, 3H, CH_3), respectively. The signal at the region 8.30–8.49 ppm is assigned to the azomethine group ($-\text{HC}=\text{N}-$). Furthermore, the ligands (HL_n) showed a broad peak in the range 9.63–9.68 ppm for OH proton of 2-hydroxy-1-naphthaldehyde ring.

3.4. X-ray diffraction

The X-ray diffraction (XRD) pattern powder forms of HL_2 and $[\text{Ru}(\text{L}_2)_2(\text{H}_2\text{O})_2]\text{Cl}$ are presented in Fig. 4. The XRD of HL_2 shows many diffraction peaks which indicate the polycrystalline phase. The average crystallite size (ξ) can be calculated from the XRD pattern according to Debye–Scherrer Eq. (9) [21,22]:

$$\xi = \frac{K\lambda}{\beta_{1/2} \cos \theta} \quad (9)$$

Table 2
The calculated quantum chemical parameters of the investigated Schiff base ligands (**HL_n**).

Comp.	E _{HOMO} (a.u)	E _{LUMO} (a.u)	ΔE (a.u)	χ (a.u)	η (a.u)	σ (a.u) ⁻¹	Pi (a.u)	S (a.u) ⁻¹	ω (a.u)	ΔN _{max}
HL₁										
(A)	-0.2689	-0.1663	0.1026	0.2176	0.0513	19.4856	-0.2176	9.7428	0.4614	4.2403
(B)	-0.3812	-0.1539	0.2273	0.2675	0.1136	8.7981	-0.2675	4.3991	0.3149	2.3538
HL₂										
(A)	-0.2694	-0.1721	0.0973	0.2207	0.0487	20.5528	-0.2207	10.2764	0.5006	4.5363
(B)	-0.3818	-0.1592	0.2226	0.2705	0.1113	8.9834	-0.2705	4.4918	0.3286	2.4301
HL₃										
(A)	-0.2694	-0.1757	0.0937	0.2226	0.0468	21.3515	-0.2225	10.6758	0.5288	4.7521
(B)	-0.3818	-0.1626	0.2192	0.2722	0.1096	9.1237	-0.2722	4.5618	0.3380	2.4836
HL₄										
(A)	-0.2691	-0.1641	0.1050	0.2166	0.0525	19.0422	-0.2165	9.5211	0.4467	4.1244
(B)	-0.3728	-0.1519	0.2209	0.2624	0.1104	9.0559	-0.2623	4.5279	0.3117	2.3761
HL₅										
(A)	-0.2707	-0.2263	0.0444	0.2485	0.0222	45.0146	-0.2484	22.5073	1.3896	11.185
(B)	-0.3822	-0.2170	0.1652	0.2996	0.0826	12.1080	-0.2996	6.0540	0.5435	3.6279

The equation uses the reference peak width at angle (θ), where λ is wavelength of X-ray radiation (1.541874 Å), K is constant taken as 0.95 for organic compounds [22] and $\beta_{1/2}$ is the width at half maximum of the reference diffraction peak measured in radians. The dislocation density, δ , is the number of dislocation lines per unit area of the crystal. The value of δ is related to the average particle diameter (ξ) by relation (10) [21,22]:

$$\delta = \frac{1}{\xi^2}. \quad (10)$$

The value of ξ is calculated and found to be 32.1 nm and the value of δ is $9.70 \times 10^{-4} \text{ nm}^{-2}$ for ligand (**HL₂**).

The diffraction peaks in powder spectra are indexed and the lattice parameters are determined with the aid of CRYSFIRE computer program [23,24]. The values of interplanar spacing (d) and Miller indices (hkl) for each diffraction peak before and after refinement are determined by using CHEKCELL program [23,24]. The values of d and corresponding hkl for **HL₂** are listed in Table 3. The results show that start 2 has orthorhombic crystal structure with space group PCA21. The lattice parameters are estimated as:

$$a = 20.1660 \text{ \AA}, \quad b = 6.8910 \text{ \AA}, \quad c = 4.5890 \text{ \AA}, \quad \alpha = \gamma = \beta = 90^\circ.$$

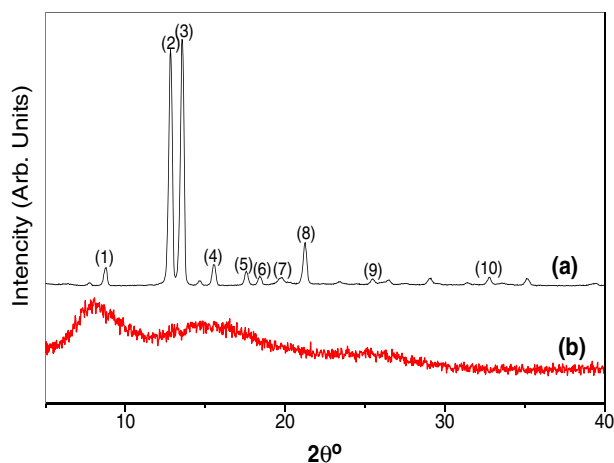


Fig. 4. X-ray diffraction (XRD) patterns powder forms of: a) ligand (**HL₂**) and b) complex (**2**).

3.5. Electronic spectra

The electronic spectra of the free ligands and the complexes were carried out in DMF solution. The free ligands showed two types of transitions, at the range 218–234 nm ($\pi-\pi^*$) transitions for the benzene ring and azomethine group and the other bands in the 285–310 nm region ($n-\pi^*$) transition of non-bonding electrons present on the nitrogen of the azomethine group. These peaks exhibited bathochromic shift upon complex formation, which supported the coordination of the ligands to Ru(III) ion. The ground state of Ru(III) in an octahedral environment is $^2T_{2g}$ and the first excited doublet levels in the order of increasing energy are $^2A_{2g}$ and $^2T_{1g}$, which arise from $t^4_{2g} e^1_g$ configuration [25]. Hence, two bands corresponding to $^2T_{2g} \rightarrow ^2A_{2g}$ and $^2T_{2g} \rightarrow ^2T_{1g}$ are possible. UV-vis spectra of the reported Ru(III) complexes show a third intense absorption band in the region 314–316 nm, which can be assigned to charge transfer (CT) transitions of the type $L_{\pi} \rightarrow ^2T_{2g}$ [26–28]. Similar observations have been made for other ruthenium(III) octahedral complexes [29,30] and in most ruthenium(III) Schiff base chelates [31].

3.6. Thermal analyses

The TGA analysis was carried out to know the actual loss of organic moiety present in the ligands **HL₁**, **HL₃** and **HL₅** and their Ru(III) complexes (**1**, **3** and **5**). It is clear that the change of substituent affects the thermal properties of the ligands and complexes. The temperature intervals and the percentage of loss of masses are listed in Table S2 in the supplementary.

The TGA curve of ligand (**HL₁**) shows two decomposition steps, the first stage occur in the temperature range 180–308 °C is attributed to loss of $C_{17}H_{12}NO$ (found 88.43% and calc. 88.80%). The second stage occurs in the temperature range 308–732 °C corresponding to loss of CH_3O (found 11.57%; calc. 11.19%).

Table 3
X-ray data of ligand (**HL₂**).

Peak no.	2θ (obs.)	2θ (calc.)	d_{hkl} (obs.)	d_{hkl} (calc.)	h k l
1	8.763	8.765	10.24	8.63	2 0 0
2	12.828	12.839	6.89	6.89	0 1 0
3	13.559	13.572	6.52	6.52	1 1 0
4	15.544	15.567	5.69	6.68	2 1 0
5	17.571	17.582	5.04	5.04	4 0 0
6	18.417	18.428	4.81	4.81	3 1 0
7	21.243	21.261	4.18	4.17	2 0 1
8	29.093	29.107	3.067	3.06	3 2 0
9	32.788	32.787	2.72	2.72	1 2 1
10	35.156	35.182	2.55	2.54	3 2 1

The ligand (HL_3) shows loss in the temperature range 190–290 °C corresponding to loss of $\text{C}_{10}\text{H}_7\text{O}$ (found 57.01%, calc. 57.8%). While the weight loss in the temperature range 290–752 °C (found 42.75%, calc. 42.11%), which is attributed to loss of a part of the ligand ($\text{C}_7\text{H}_6\text{N}$).

TG curve of the (HL_5) ligand shows three steps of decomposition. The first stage of decomposition occur in the temperature range of 120–331 °C and are associated with the loss of a part of the ligand (C_7H_6) with an estimated weight loss of 30.95% (calcd. 30.82%). The second stage of decomposition occur in the temperature range of 331–760 °C and are associated with the loss of $\text{C}_9\text{H}_6\text{N}_2\text{O}_3$ atoms and with an estimated weight loss of 64.88% (calcd. 65.07%). The finally stage of decomposition associated with the loss of 4C atoms with an estimated weight loss of 4.20% (calcd. 4.11%).

All Ru(III) complexes showed TG curves in the temperature range ~100–209 °C loss of coordinated water molecules. The second and third stages are related to loss of a part of the ligand. The final weight losses are due to the decomposition of the rest of the ligand leaving metal oxides residue (Table S2 in the supplementary).

3.6.1. Calculation of activation thermodynamic parameters

The thermodynamic activation parameters of decomposition processes of the ligands (HL_1 , HL_3 and HL_5) and their Ru(III) complexes (**1**, **3** and **5**) namely activation energy (E_a), enthalpy (ΔH^*), entropy (ΔS^*), and Gibbs free energy change of the decomposition (ΔG^*) are evaluated graphically by employing the Coast–Redfern [32] and Horowitz–Metzger [33] methods.

3.6.1.1. Coast–Redfern equation. The Coast–Redfern Eq. (11), which is a typical integral method, can represent as:

$$\int_0^{\alpha} \frac{dx}{(1-\alpha)^n} = \frac{A}{\varphi} \int_{T_1}^{T_2} \exp\left(-\frac{E_a}{RT}\right) dt. \quad (11)$$

For convenience of integration, the lower limit T_1 usually taken as zero. This equation on integration gives:

$$\ln\left[-\frac{\ln(1-\alpha)}{T^2}\right] = -\frac{E_a}{RT} + \ln\left[\frac{AR}{\varphi E_a}\right]. \quad (12)$$

A plot of left-hand side (LHS) against $1/T$ was drawn (Fig. 5). E_a is the energy of activation in J mol^{-1} and calculated from the slope and A in (s^{-1}) from the intercept value. The entropy of activation (ΔS^*) in ($\text{J mol}^{-1} \text{K}^{-1}$) calculated by using Eq. (13):

$$\Delta S^* = 2.303 \left[\log\left(\frac{Ah}{k_B T_s}\right) \right] R \quad (13)$$

where k_B is the Boltzmann constant, h is the Plank's constant and T_s is the TG peak temperature.

3.6.1.2. Horowitz–Metzger equation. The Horowitz–Metzger equation is an illustrative of the approximation methods. These authors derived the relation:

$$\log\left[\frac{1-(1-\alpha)^{1-n}}{1-n}\right] = \frac{E_a \theta}{2.303RT_s^2} \quad \text{for } n \neq 1 \quad (14)$$

when $n = 1$, the LHS of Eq. (14) would be $\log[-\log(1-\alpha)]$ (Fig. 6). For a first order kinetic process, the Horowitz–Metzger equation may write in the form:

$$\log\left[\log\left(\frac{W_\alpha}{W_\gamma}\right)\right] = \frac{E_a \theta}{2.303RT_s^2} - \log 2.303 \quad (15)$$

where $\theta = T - T_s$, $w_\gamma = w_\alpha - w$, $w_\alpha =$ mass loss at the completion reaction; $w =$ mass loss up to time t . The plot of $\log[\log(w_\alpha/w_\gamma)]$ vs.

θ was drawn and found to be linear from the slope of which E_a was calculated. The pre-exponential factor, A , calculated from Eq. (16):

$$\frac{E_a}{RT_s^2} = \frac{A}{\left[\varphi \exp\left(-\frac{E_a}{RT_s}\right)\right]}. \quad (16)$$

The entropy of activation, ΔS^* , is calculated from Eq. (13). The enthalpy activation, ΔH^* , and Gibbs free energy, ΔG^* , calculated from:

$$\Delta H^* = E_a - RT \quad (17)$$

$$\Delta G^* = \Delta H^* - T\Delta S^*. \quad (18)$$

The calculated values of E_a , A , ΔS^* , ΔH^* and ΔG^* for the decomposition steps for ligands (HL_1 , HL_3 and HL_5) and their Ru(III) complexes (**1**, **3** and **5**) are summarized in Table 4. The kinetic data obtained from the two methods are comparable and can be considered in good agreement with each other. The entropy of activation energies reflects the thermal stability of the compounds. The entropy of activation is found to be of negative values in the ligands (HL_n) and their Ru(III) complexes (**1**, **3** and **5**) which indicate that the decomposition reactions proceed spontaneously [34,35]. The values of ΔG^* are positive considered as favorable or spontaneous reaction. The values of ΔH^* are positive indicate that the reaction is endothermic.

From the values of the energy of activation (E_a) of the ligands (HL_n) and their Ru(III) complexes (**1**, **3** and **5**), it is observed that all the Ru(III) complexes are less stable than the ligands (HL_n). As shown in Fig. S2 in the supplementary, the E_a values for the ligand (HL_5) and its Ru(III) complex (**5**) is higher values compared to the other compounds. This can be attributed to the fact that the effective charge increased due to the electron withdrawing p -substituent (HL_5) while it decreased by the electrons donating character of (HL_1). This is in accordance with that expected from Hammett's constant (σ^R) (Fig. S2).

3.7. Catalytic oxidation of benzoin

The catalytic activity of ruthenium complexes for the oxidation of benzoin to benzil has been studied and the effect of time, solvent and temperature were optimized to produce maximum yield. The electronic spectrum of benzil is characterized by absorption at 305 nm, which is readily differentiated from the absorption bands of benzoin at 247 nm [36]. Accordingly, the band at 305 nm was used to determine the concentration of the produced benzil. Three ruthenium(III) complexes (**1**, **3** and **5**) were tested as catalyst for oxidation of benzoin using NaO_4 as an oxidant under different reaction conditions viz., temperature, reaction time and type of solvent in order to optimize the conditions to find out the best catalyst.

The absorbance at 305 nm increases with reaction time as an indication of the increasing concentration of benzil by using one of the catalysts, complex (**5**). The maximum benzil yield was found to depend on the type of catalyst used. It is clear from Fig. 7 that complex (**5**) and complex (**3**) give higher benzil yields than complex (**1**) with the same reaction time. Complex (**3**) gave 50% yield after 2 h, while complex (**5**) gave 68% after a longer reaction time (4 h). The order of catalytic activity was found to be as follows: complex (**5**) > complex (**3**) > complex (**1**). It was found that the values of yield (%) and TOF values are related to the nature of the p -substituent as they increase according to the following order $p\text{-NO}_2 > \text{H} > \text{OCH}_3$. This can be attributed to the fact that the effective charge increased due to the electron withdrawing p -substituent (HL_5) while it decreased by the electrons donating character of (HL_1). This is in accordance with that expected from Hammett's constant (σ^R) as shown in Fig. S3 in the supplementary. Correlation of the yield (%) and TOF values Hammett's constant (σ^R) showed the incensement of these values with increasing σ^R .

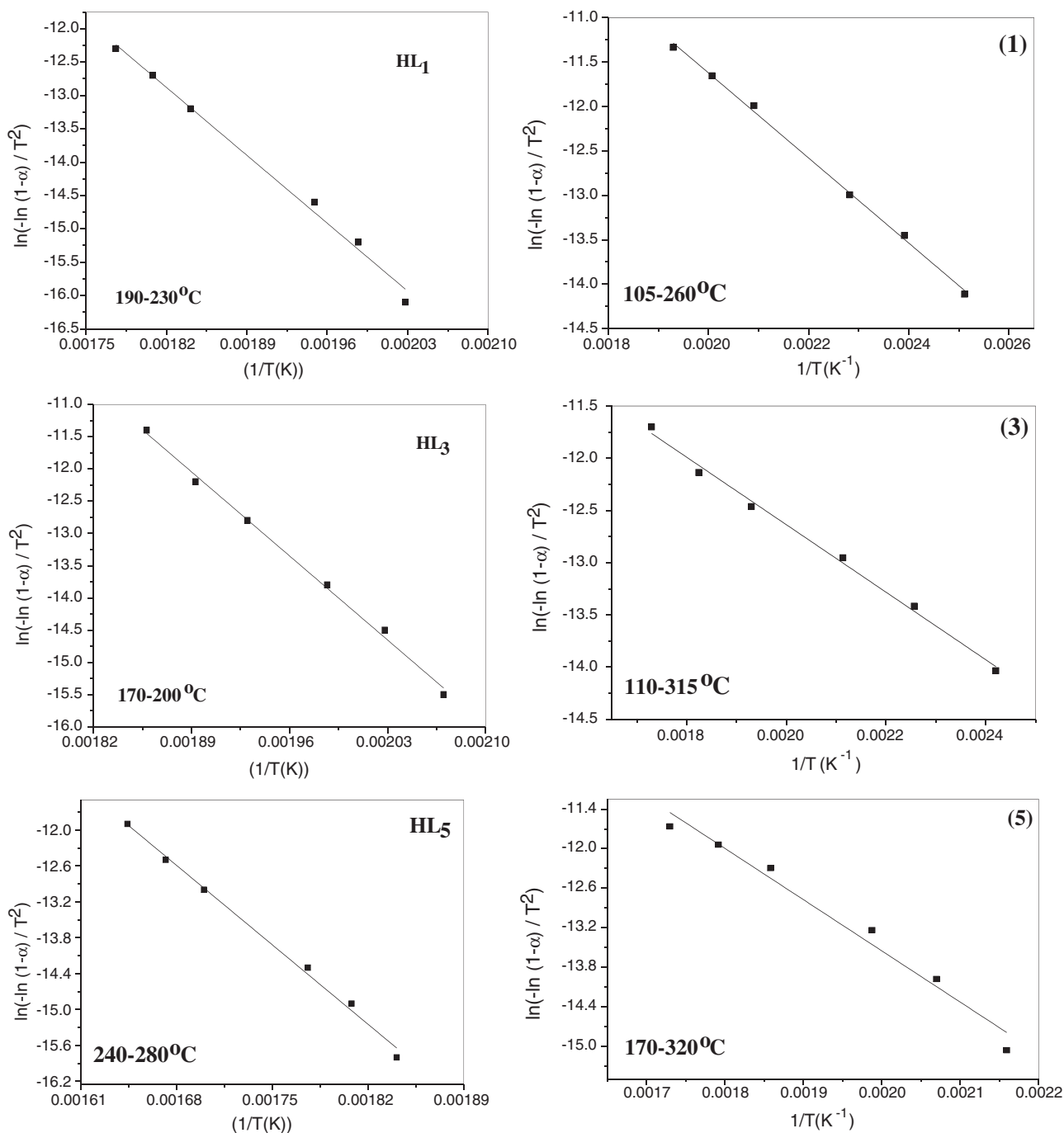


Fig. 5. Coats-Redfern (CR) of the ligands (**HL**₁, **HL**₃ and **HL**₅) and their Ru(III) complexes (**1**, **3** and **5**).

3.7.1. Effect of solvent

The influence of three different solvents viz. benzene, toluene and acetonitrile on the yield of benzoin oxidation was studied using the complexes **1**, **3** and **5**.

3.7.2. Effect of temperature

The performance of the catalysts was investigated at three different temperatures viz. 30, 50 and 70 °C in acetonitrile after 3 h reaction time (Table S3 in the supplementary). In general, the catalytic activity of the three catalysts increased with increasing temperature. Fig. 7 showed that there was a significant increase in benzil yield using complexes

(**1**), (**3**) and (**5**) when the reaction temperature was increased from 30 to 70 °C. At 30 °C, moderate yields of benzil were obtained. However, increasing the temperature to 70 °C led to increasing the yield to 70% of benzil. This indicates that at 70 °C the best yield was obtained under these reaction conditions.

3.7.3. Effect of time

The catalytic oxidation of benzoin using NaIO₄ as oxidant in the presence of the three complexes was followed as a function of time in acetonitrile at 70 °C. The reaction profiles showed that the yield of benzil increased with increasing reaction time until a steady state was reached after 4 h (Fig. 8).

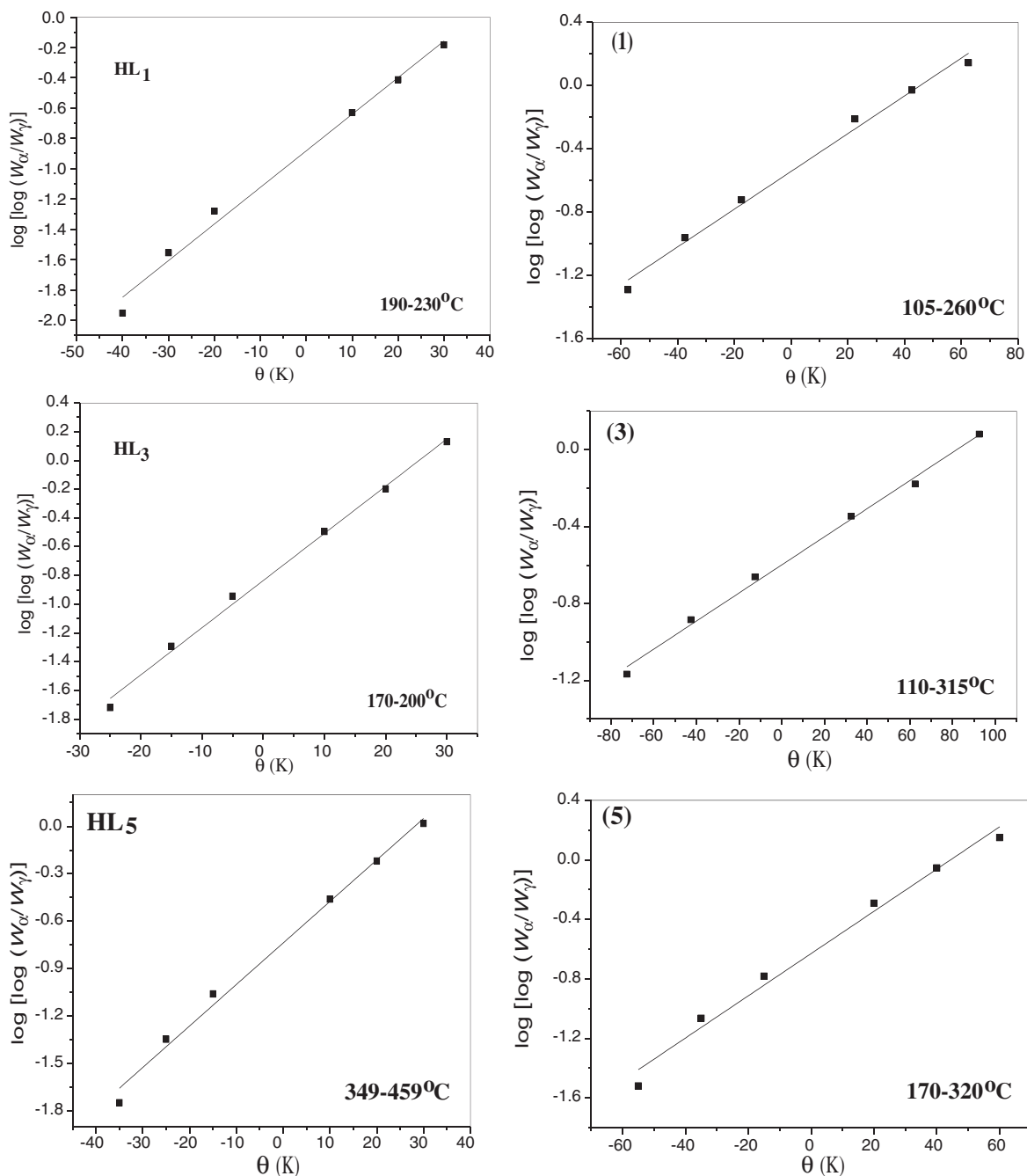


Fig. 6. Horowitz–Metzger (HM) of the ligands (**HL₁**, **HL₃** and **HL₅**) and their Ru(III) complexes (**1**, **3** and **5**).

3.7.4. The mechanism for the catalytic oxidation of benzoin to benzil by $[\text{Ru}(\text{L}_n)_2(\text{H}_2\text{O})_2]\text{Cl}/\text{NaIO}_4$

The oxidation of alcohols to the corresponding carbonyl compound is well-known to take place by high-valent metal oxo complexes. Therefore, The catalytic oxidation of benzoin to benzil by $[\text{Ru}(\text{L}_n)_2(\text{H}_2\text{O})_2]\text{Cl}/\text{NaIO}_4$ could be achieved via high valent ruthenium oxo species [37]. The hydride abstraction mechanism is suggested here for the process of catalytic oxidation of benzoin to benzil by the new Schiff base ruthenium(III) complexes. An accurate mechanistic study for reactions containing low-valent ruthenium complexes as catalysts suggests the formation of metal-oxo intermediates [38]. The complex $[\text{Ru}(\text{L}_n)_2(\text{H}_2\text{O})_2]\text{Cl}$ reacts with NaIO_4 to produce $[\text{RuO}^{\text{V}}(\text{L}_1)_2(\text{H}_2\text{O})]^{2+}$, NaIO_3 and water (Eq. (19)). Association of benzoin to the resulting ruthenium oxo complex occurs,

followed by hydride abstraction to form the unstable intermediate, $[\text{RuO}^{\text{V}}(\text{L}_1)_2\text{HOCHPhCOPh}(\text{H}_2\text{O})]^{+}$ (Eq. (20)). This intermediate loses water molecule which in turn associates with ruthenium ion to yield benzil, and the starting complex to complete the catalytic cycle (Eqs. (21) and (22)). This catalytic cycle continues until all the benzoin completely consumed as shown in Fig. 9.

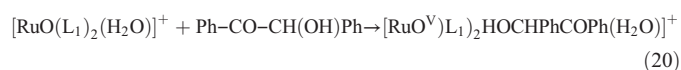
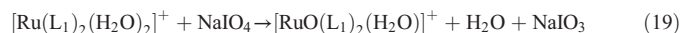
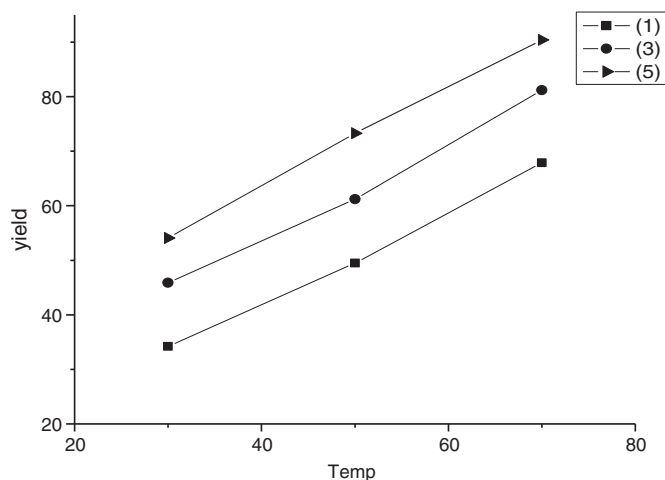
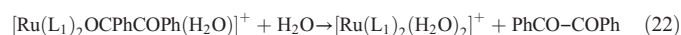
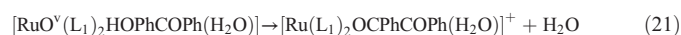
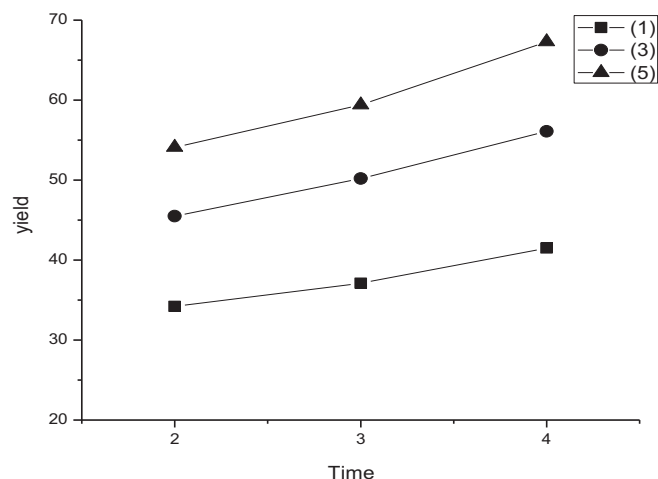


Table 4The kinetic parameters of the Schiff base ligands (**HL**₁, **HL**₃ and **HL**₅) and their Ru(III) complexes (**1**, **3** and **5**).

Compound ^a	Decomp. temp. (°C)	Method	Parameter					Correlation coefficient (r)
			E _a (kJ mol ⁻¹)	A (s ⁻¹)	ΔS [*] (J mol ⁻¹ K ⁻¹)	ΔH [*] (kJ mol ⁻¹)	ΔG [*] (kJ mol ⁻¹)	
HL ₁	190–230	CR	121	1.94E+09	-7.20E+01	116	155	0.98146
		HM	132	7.36E+10	-4.17E+0	127	149	0.98894
(1)	105–260	CR	39.8	1.04E+02	-2.10E+02	36.1	132	0.99772
		HM	47.4	1.25E+03	-1.89E+02	43.6	130	0.98986
HL ₃	170–200	CR	155	3.56E+13	1.01E+01	151	146	0.99581
		HM	162	6.11E+14	3.37E+01	158	141	0.9952
(3)	110–315	CR	26.9	1.12E+00	-2.48E+02	22.8	143	0.99396
		HM	33.0	9.97E+00	-2.30E+02	29.0	141	0.99478
HL ₅	240–280	CR	157	7.02E+11	-2.36E+01	135	166	0.99392
		HM	168	1.56E+13	2.17E+00	163	162	0.99104
(5)	170–320	CR	64.7	9.68E+03	-1.73E+02	60.4	150	0.97074
		HM	72.9	1.23E+05	-1.52E+02	68.6	147	0.98316

^a Numbers as given in Table 1.**Fig. 7.** Effect of temperature on benzil yield using complexes (**1**, **3** and **5**) as a catalyst.**Fig. 8.** Effect of time on benzil yield using complexes (**1**, **3** and **5**) as a catalyst.

3.8. Antibacterial studies

The antimicrobial activity of ligands (**HL**_n) and their Ru(III) complexes was tested against bacteria and fungi; we used more than one test organism to increase the chance of detecting their antimicrobial activities. The organisms used in the present investigations included two Gram positive bacteria (*B. cereus* and *S. aureus*) and two Gram negative bacteria (*E. coli* and *K. pneumoniae*) in addition to different kinds of fungi (*A. niger*, *F. oxysporium*, *P. italicum* and *A. alternata*).

The results of the antibacterial activity of ligands (**HL**_n) and their ruthenium(III) complexes (**1–5**) are tested against bacterial species as shown in Table 5. The ligand **HL**₃ has antibacterial activity against *B. cereus* (inhibition zone of **HL**₃ = 8 and 7 mm at concentrations = 100 and 150 μg/ml, respectively) and *S. aureus* (inhibition zone of **HL**₃ = 4 and 5 mm at concentrations = 100 and 150 μg/ml, respectively), but low or no effects were recorded against Gram negative bacteria. For the complexes, all of them were found to have high antibacterial activity against Gram positive bacteria namely; *B. cereus* (inhibition zone of complex **(1)** = 8 and 10 mm at concentrations = 50 and 100 μg/ml, respectively; inhibition zone of complex **(3)** = 7 and 10 mm at concentrations = 50 and 100 μg/ml, respectively) and *S. aureus* (inhibition zone of complex **(1)** = 4 and 6 mm at concentrations = 100 and 150 μg/ml, respectively) when comparing with penicillin except complex **(5)**.

Ligands **HL**₁, **HL**₂, **HL**₃, **HL**₄ and **HL**₅ and complexes (**1–5**) have no effect against *B. cereus*, *S. aureus*, *E. coli* and *K. pneumoniae* when comparing with penicillin.

Comparative analysis for antibacterial study of ligands (**HL**_n) and their ruthenium(III) complexes (**1–5**) is shown in Fig. S4 in the supplementary. It is observed that the ligand (**HL**₃) and all complex are more potent antibacterial than other ligands against *B. cereus* and *S. aureus*. This may support the argument that some type of biomolecular binding

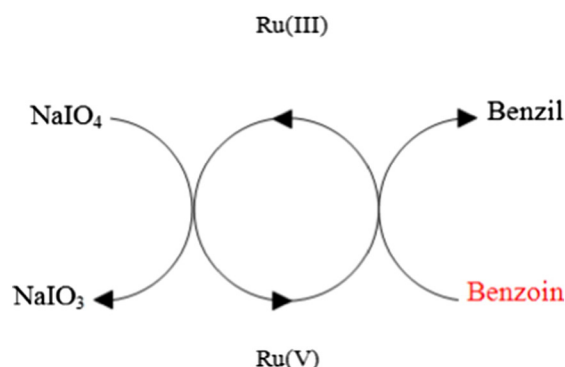
**Fig. 9.** Mechanism for oxidation of benzoin to benzil by $[\text{Ru}(\text{L}_n)_2(\text{H}_2\text{O})_2]\text{Cl}/\text{NaIO}_4$.

Table 5
Antibacterial activity data of Schiff base ligands (**HL_n**) and their Ru(III) (**1–5**). The results were recorded as the diameter of inhibition zone (mm).

Compound ^a	Conc. (µg/ml)	Gram positive bacteria		Gram negative bacteria	
		<i>Bacillus cereus</i>	<i>Staphylococcus aureus</i>	<i>Escherichia coli</i>	<i>Klebsiella pneumoniae</i>
HL₁	50	–ve	–ve	–ve	–ve
	100	–ve	–ve	–ve	–ve
	150	–ve	–ve	–ve	–ve
HL₂	50	–ve	–ve	–ve	–ve
	100	–ve	–ve	–ve	–ve
	150	–ve	–ve	–ve	–ve
HL₃	50	8	3	1	–ve
	100	8	4	–ve	–ve
	150	7	5	–ve	–ve
HL₄	50	–ve	–ve	1	–ve
	100	–ve	–ve	1	–ve
	150	3	–ve	1	1
HL₅	50	–ve	–ve	–ve	–ve
	100	–ve	–ve	–ve	–ve
	150	–ve	–ve	–ve	–ve
(1)	50	8	4	–ve	1
	100	10	4	–ve	1
	150	11	6	1	1
(2)	50	6	4	–ve	–ve
	100	9	6	2	1
	150	9	7	2	1
(3)	50	7	4	–ve	1
	100	10	4	–ve	1
	150	10	6	–ve	1
(4)	50	8	4	–ve	–ve
	100	7	6	1	2
	150	11	6	2	2
(5)	50	2	2	–ve	–ve
	100	3	2	–ve	–ve
	150	4	2	–ve	–ve
Penicillin	50	1	2	1	–ve
	100	3	2	3	–ve
	150	3	2	3	–ve

^a Numbers as given in Table 1.

to the metal ions or interchelation or electrostatic interactions causes the inhibition of biological synthesis [39].

The results of the antifungal activity of ligands (**HL_n**) and their ruthenium(III) complexes are listed in Table 6. The results of the examination of antifungal activity revealed that *A. niger* is resistant to all ligands and complexes when compared with Miconazole. **HL_n** ligands and complexes are moderately effective against *F. oxysporum* (inhibition zone of **HL₃** (4 and 4 mm) at concentrations (100 and 150 µg/ml), respectively) (Table 6). Complex (**1**) showed good effect against *P. italicum* (inhibition zone of (**1**)) (4 and 4 mm) at concentrations (50 and 100 µg/ml respectively) when compared with Miconazole. Complexes (**2–5**) have no effect against *P. italicum*. The enhancement in antifungal activity is rationalized on the basis of the partial sharing of the positive charge of metal ions with donor groups [40]. So it can be concluded that some complexes exhibits higher antimicrobial activity than the free ligand [41].

4. Conclusion

Five novel ruthenium(III) complexes of the Schiff base ligands have been synthesized and structurally characterized. Based on elemental analysis, molar conductivity, UV–vis, magnetic, spectral data and thermal analysis, mononuclear octahedral complexes of the general formula [Ru(**L_n**)₂(H₂O)₂]Cl are proposed, where **L** = monoanion of the bidentate Schiff base ligand. The optimized bond lengths, bond angles and calculated the quantum chemical parameters for the ligands (**HL_n**) were investigated. The thermogravimetric analysis of the ligands showed that the values of activation energies of decomposition (*E_a*) are found to be 121, 155 and 157 kJ/mol for the ligands **HL₂**, **HL₃** and **HL₅**, respectively. The values of *E_a* are found to be 39.8, 26.9 and

Table 6
Antifungal activity data of Schiff base ligands (**HL_n**) and their Ru(III) complexes (**1–5**). The results were recorded as the diameter of inhibition zone (mm).

Compound ^a	Conc. (µg/ml)	<i>Aspergillus niger</i>	<i>Fusarium oxysporum</i>	<i>Alternaria alternata</i>	<i>Penicillium italicum</i>
HL₁	50	–ve	–ve	–ve	–ve
	100	–ve	2	–ve	–ve
	150	–ve	2	–ve	–ve
HL₂	50	–ve	2	–ve	–ve
	100	–ve	2	–ve	–ve
	150	–ve	2	2	–ve
HL₃	50	–ve	1	–ve	2
	100	–ve	4	3	2
	150	–ve	4	–ve	2
HL₄	50	–ve	1	3	–ve
	100	–ve	1	–ve	–ve
	150	–ve	1	–ve	–ve
HL₅	50	–ve	1	3	–ve
	100	–ve	1	3	–ve
	150	–ve	1	1	–ve
(1)	50	–ve	1	1	4
	100	–ve	2	3	4
	150	–ve	2	3	–ve
(2)	50	–ve	2	3	–ve
	100	–ve	2	–ve	–ve
	150	–ve	5	–ve	–ve
(3)	50	–ve	1	–ve	–ve
	100	–ve	2	5	–ve
	150	–ve	3	5	–ve
(4)	50	–ve	3	3	–ve
	100	–ve	3	4	–ve
	150	–ve	3	4	–ve
(5)	50	–ve	3	–ve	–ve
	100	–ve	3	–ve	–ve
	150	–ve	3	–ve	–ve
Miconazole	50	1	2	5	1
	100	3	3	6	1
	150	4	3	6	2

^a Numbers as given in Table 1.

64.7 kJ/mol for the complexes **1**, **3** and **5**, respectively. These complexes were found to be effective catalyst for the oxidation of benzoin to benzil in the presence of NaIO₄ as co-oxidant. The antifungal activity of all the ligands (**HL_n**) and their Ru(III) complexes (**1–5**) were investigated. It was found that the ligand (**HL₃**) has the best antibacterial activity (*S. aureus* and *B. cereus*) and all Ru(III) complexes have higher antifungal activity than the ligands against *F. oxysporum*.

Acknowledgements

The authors would like to thank Prof. M.I. Abou-Dobara and Miss. N.F. Omar (Botany Department, Faculty of Science, Damietta University, Egypt) for their help during testing antibacterial activity.

Appendix A. Supplementary data

Supplementary data to this article can be found online at <http://dx.doi.org/10.1016/j.molliq.2015.07.001>.

References

- [1] A.A. Abou-Hussein, W. Linert, Spectrochim. Acta A 117 (2014) 763–771.
- [2] F. Ricci, A.J. Bonham, A.C. Mason, N.O. Reich, K.W. Plaxco, Anal. Chem. 81 (2009) 1608–1614.
- [3] L. Lekha, K.K. Raja, G. Rajagopal, D. Easwaramoorthy, J. Mol. Struct. 1056 (2014) 307–313.
- [4] G. Prakash, R. Manikandan, P. Viswanathamurthi, K. Velmurugan, R. Nandhakumar, J. Photochem. Photobiol. B Biol. 138 (2014) 63–74.
- [5] C.M. Metzler, A. Cahill, D.E. Metzler, J. Am. Chem. Soc. 102 (1980) 6075–6082.
- [6] A.M. El-Naggar, F.S.M. Ahmed, M.F. Badie, J. Heterocycl. Chem. 18 (1981) 91–94.
- [7] M. Hayvali, Z. Hayavali, Met. Org. Chem. 34 (2004) 713–732.
- [8] A.F. Shoair, Bull. Korean Chem. Soc. 26 (2005) 1525–1528.
- [9] A.F. Shoair, R.H. Mohamed, Synth. Commun. 36 (2006) 59–64.
- [10] A.F. Shoair, J. Coord. Chem. 60 (2007) 1101–1108.

- [11] A.F. Shoair, R.H. Mohamed, *J. Coord. Chem.* 60 (2007) 1279–1289.
- [12] J. Matijević-Sosa, M. Vinković, D. Vikić-Topić, *Croat. Chem. Acta* 79 (2006) 489–495.
- [13] A.F. Shoair, A.A. El-Bindary, *Spectrochim. Acta A* 131 (2014) 490–496.
- [14] M.M. Bekheit, A.R. El-Shobaky, M.T. Gad Allah, *Arab. J. Chem.* (2013) <http://dx.doi.org/10.1016/j.arabj.2013.07.025>.
- [15] A.F. Shoair, A.R. El-Shobaky, E.A. Azab, *J. Mol. Liq.* 203 (2015) 59–65.
- [16] M.A. Diab, A.Z. El-Sonbati, A.A. El-Bindary, G.G. Mohamed, *Res. Chem. Intermed.* (2015) <http://dx.doi.org/10.1007/s11164-015-1946-0>.
- [17] S. Pal, S. Pal, *J. Chem. Soc. Dalton Trans.* 2002 (2002) 2102–2108.
- [18] M. Amirnasr, A.H. Mahmoudkhani, A. Gorji, S. Dehghanpour, H.R. Bijanzadeh, *Polyhedron* 21 (2002) 2733–2742.
- [19] K. Nakamoto, *Infrared and Raman Spectra of Inorganic and Coordination Compounds*, Wiley-Interscience, New York, 1971.
- [20] A.A. El-Bindary, *Transit. Met. Chem.* 22 (1997) 381–384.
- [21] A.A. El-Bindary, A.Z. El-Sonbati, M.A. Diab, Sh.M. Morgan, *J. Mol. Liq.* 201 (2015) 36–42.
- [22] N.A. El-Ghamaz, A.Z. El-Sonbati, M.A. Diab, A.A. El-Bindary, G.G. Mohamed, Sh.M. Morgan, *Spectrochim. Acta A* 147 (2015) 200–211.
- [23] N.A. El-Ghamaz, M.A. Diab, A.A. El-Bindary, A.Z. El-Sonbati, H.A. Seyam, *J. Mater. Sci. Semicond. Process.* 27 (2014) 521–531.
- [24] E.M. El-Menyawy, N.A. El-Ghamaz, H.H. Nawar, *J. Mol. Struct.* 1036 (2013) 144–150.
- [25] C.J. Balhausen, *Ligand Field Theory*, McGraw-Hill, New York, 1962.
- [26] K. Chichak, U. Jacquemard, N.R. Branda, *Eur. J. Inorg. Chem.* 2002 (2002) 357–368.
- [27] R. Samanta, B. Mondal, P. Munshi, G.K. Lahiri, *J. Chem. Soc. Dalton Trans.* 2001 (2001) 1827–1833.
- [28] G. Venkatachalam, N. Raja, D. Pandiarajan, R. Ramesh, *Spectrochim. Acta A* 71 (2008) 884–891.
- [29] N. Padma Priya, S. Arunachalam, A. Manimaran, D. Muthupriya, C. Jayabalakrishnan, *Spectrochim. Acta A* 72 (2009) 670–676.
- [30] M. Muthukumar, P. Viswanathamurthi, R. Prabhakaran, K. Natarajan, *J. Coord. Chem.* 63 (2010) 3833–3848.
- [31] R. Ramesh, S. Maheswaran, *J. Inorg. Biochem.* 96 (2003) 457–462.
- [32] A.W. Coats, J.P. Redfern, *Nature* 20 (1964) 68–79.
- [33] H.W. Horowitz, G. Metzger, *Anal. Chem.* 35 (1963) 1464–1468.
- [34] A.Z. El-Sonbati, M.A. Diab, A.A. El-Bindary, G.G. Mohamed, Sh.M. Morgan, *Inorg. Chim. Acta* 430 (2015) 96–107.
- [35] A.Z. El-Sonbati, M.A. Diab, A.A. El-Bindary, A.M. Eldesoky, Sh.M. Morgan, *Spectrochim. Acta A* 135 (2015) 774–791.
- [36] M.R. Maurya, S. Sikarwar, P. Manikandan, *Appl. Catal. A* 315 (2006) 74–82.
- [37] R.A. Sheldon, J.K. Kochi, *Metal Catalyzed Oxidation of Organic Compounds*, Academic Press, New York, 1981. (Chapt. 6).
- [38] I.N. Booyesen, S. Maikoo, M.P. Akerman, B. Xulu, *Polyhedron* 79 (2014) 250–257.
- [39] Z.H. Chohan, K.M. Khan, C.T. Supuran, *Appl. Organomet. Chem.* 18 (2004) 305–310.
- [40] N. Dharmaraj, P. Viswanathamurthi, K. Natarajan, *Transit. Met. Chem.* 26 (2001) 105–109.
- [41] P.K. Panchal, P.B. Pansuria, M.N. Patel, *J. Enzyme Inhib. Med. Chem.* 21 (2006) 203–209.